

# Supporting Information

## Nitroxide Derivatives for Dynamic Nuclear Polarization in Liquids: the Role of Rotational Diffusion

M. Levien<sup>a,b</sup>, M. Hiller<sup>a</sup>, I. Tkach<sup>a</sup>, M. Bennati<sup>a,b</sup>, T. Orlando<sup>a</sup>

<sup>a</sup>*Research Group EPR Spectroscopy, Max Planck Institute for Biophysical Chemistry, Göttingen, Germany*

<sup>b</sup>*Department of Chemistry, Georg-August University, Göttingen, Germany*

### Contents

<b>S1</b>	<b>SAMPLE PREPARATION</b>	<b>2</b>
<b>S2</b>	<b>CW-EPR MEASUREMENTS</b>	<b>2</b>
<b>S3</b>	<b>DIFFUSION COEFFICIENT</b>	<b>2</b>
S3.1	Toluene . . . . .	4
S3.2	Chloroform . . . . .	4
<b>S4</b>	<b>GEOMETRY OPTIMIZATION FOR TL/TOLUENE COMPLEX</b>	<b>4</b>
<b>S5</b>	<b><sup>1</sup>H-DNP MEASUREMENTS AT 0.34 T</b>	<b>6</b>
S5.1	Saturation factor . . . . .	6
S5.2	Leakage factor and $T_{\text{Build-up}}$ . . . . .	6
S5.3	NMR enhancement . . . . .	7
<b>S6</b>	<b><sup>1</sup>H-COUPPLING FACTOR <math>\xi_{1\text{H}}</math></b>	<b>7</b>
S6.1	Experimental data . . . . .	7
<b>S7</b>	<b><sup>13</sup>C-DNP MEASUREMENTS</b>	<b>10</b>
<b>S8</b>	<b>RELAXATION MODEL FOR <math>\xi</math></b>	<b>10</b>
<b>S9</b>	<b>SIMULATIONS OF <math>\xi_{1\text{H}}</math></b>	<b>11</b>
<b>S10</b>	<b>SIMULATIONS OF <math>\xi_{13\text{C}}</math></b>	<b>12</b>
<b>S11</b>	<b>DFT AND MD SIMULATIONS OF TEMPONE AND FN-2a</b>	<b>14</b>
S11.1	DFT calculations . . . . .	14
S11.2	MD parameters and simulations . . . . .	14
S11.2.1	Partial charges . . . . .	14
S11.2.2	Bond, angle and non-bonding parameters . . . . .	17
S11.2.3	System setup, equilibration and simulation details . . . . .	19

## S1 SAMPLE PREPARATION

Nitroxide radical 4-Hydroxy-2,2,6,6-tetramethylpiperidine 1-oxyl, known as TEMPOL, was purchased from Sigma-Aldrich, as well as 3 $\beta$ -DOXYL-5 $\alpha$ -cholestane (TP-CLST). 4-Oxo-2,2,6,6-tetramethylpiperidine-d<sub>16</sub>, 1-<sup>15</sup>N-1-oxyl (<sup>15</sup>N-TEMPONE-d<sub>16</sub>) was purchased from Sigma-Aldrich. <sup>13</sup>C-labelled chloroform and tetrachlormethane were purchased from Eurisotop and Sigma-Aldrich, respectively. Toluene and chloroform were purchased from Merck KGaA. Fullerene-nitroxides (FN) were synthesized in house as described in Ref. [6]. Radical concentration ranges from 0.5 mM to 1.5 mM and from 3 mM to 20 mM (Table S.I) for <sup>1</sup>H DNP measurements at 0.34 T and <sup>13</sup>C DNP measurements at 1.2 T, respectively and was calibrated by CW-EPR spin counting. About 7  $\mu$ L of sample was inserted in a quartz tube with outer diameter of 1.6 mm and inner diameter of 0.8 mm. Samples were then degassed by freeze-pump-thaw cycles (from one to three) to remove the oxygen dissolved inside. Due to the degassing procedure, the error of the concentration of the polarizer used is around 15 %.

## S2 CW-EPR MEASUREMENTS

EPR spectra are acquired at 9.4 GHz/0.34 T (modulation amplitude 0.1 mT, modulation frequency 100 kHz) on degassed samples (Figure S2 and S3). The molecular rotational correlation time  $\tau_c^{\text{EPR}}$  was obtained by fitting the data with Easyspin [30], using the routine *garlic* (for TEMPOL and TP-CLST) and *chili* (for FNs samples), corresponding to the fast motion and the slow motions regime, respectively. In the case of FN samples, the rigid linker restricts the motion of the nitroxide radical and assure that the FN molecule rotates as a whole. As simulation parameters we assumed  $g = [2.0090, 2.0065, 2.0022]$  and  $A = [16.9, 19.1, 93.7]$ , the latter with a 10% deviation allowed to improve the fit quality for different solvent and polarizing agents, whereas the adjusted fit parameters were kept unchanged within the whole temperature range.  $\tau_c^{\text{EPR}}$  shows a clear trend as a function of the temperature in both toluene and chloroform, which can be fitted with an exponential decay, i.e.  $\tau_c^{\text{EPR}} = \tau_0^{\text{EPR}} + A \cdot \exp(-E/T)$  (Figure S4). The rotational correlation times of nitroxide derivatives at room temperature are listed in Table S.I, while some of the spectra are shown in Figure S3.

## S3 DIFFUSION COEFFICIENT

Diffusion coefficients of the solvents and the radical in the solvent were measured by PFG (pulsed field gradient) NMR [14]. Measurements were performed on a 400 MHz Bruker UltraShield Avance III HD spectrometer using a 5 mm PAQXI 1H/31P-13C/15N Z-GRD 1832842/0001 probehead. The maximum gradient duration was 2.7 ms using a maximum gradient strength of 0.385 T/m. Experiments were carried out utilizing the standard Bruker pulse sequence dstebpgp3s introduced by Jerschow and Müller [14]. A gradient recovery delay of 0.5 ms was used and the diffusion time was up to 50 ms. Samples were measured in a 5 mm tube. Measurements were performed in the temperature range 190 – 310 K, using a liquid nitrogen cooling cabinet for  $T < 260$  K and a dry nitrogen gas flow for  $T > 260$  K.

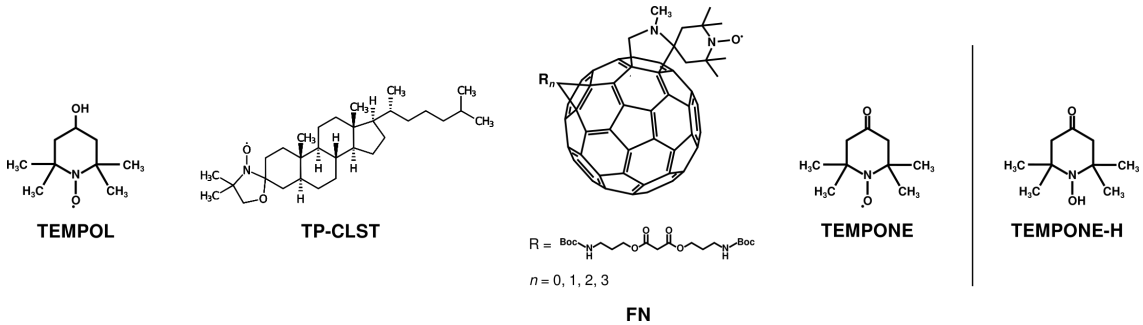


Figure S1: Structures of the nitroxide derivatives used as polarizing agents and the reduced form of TP used for diffusion measurements (TEMPONE-H).

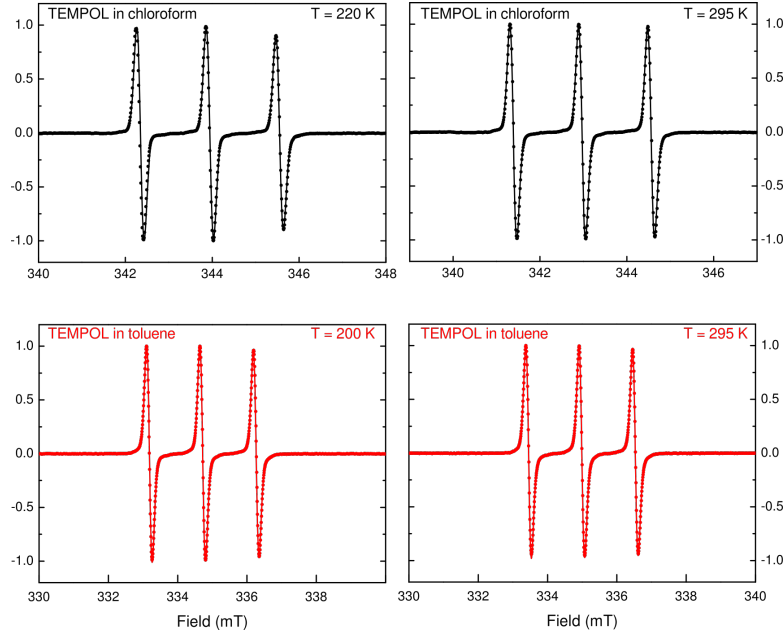


Figure S2: CW-EPR spectra obtained at 9.4 GHz of TEMPOL in chloroform (black) and toluene (red) at two characteristic temperatures. Fit (solid lines) were performed with *garlic* (fast motions regime) routine in Easyspin [30].

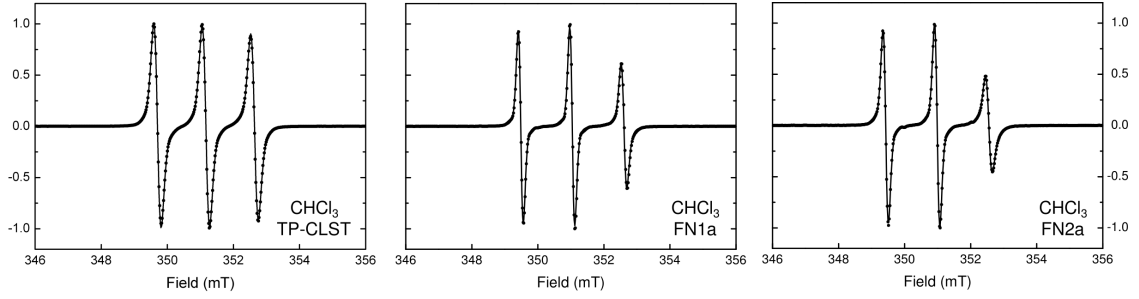


Figure S3: CW-EPR spectra obtained at 9.4 GHz of different polarizing agents in chloroform at room temperature. Fit (solid lines) were performed in Easyspin [30] with *garlic* routine (fast motions regime) for TP-CLST radical and with *chili* routine (slow motions regime) for FN samples.

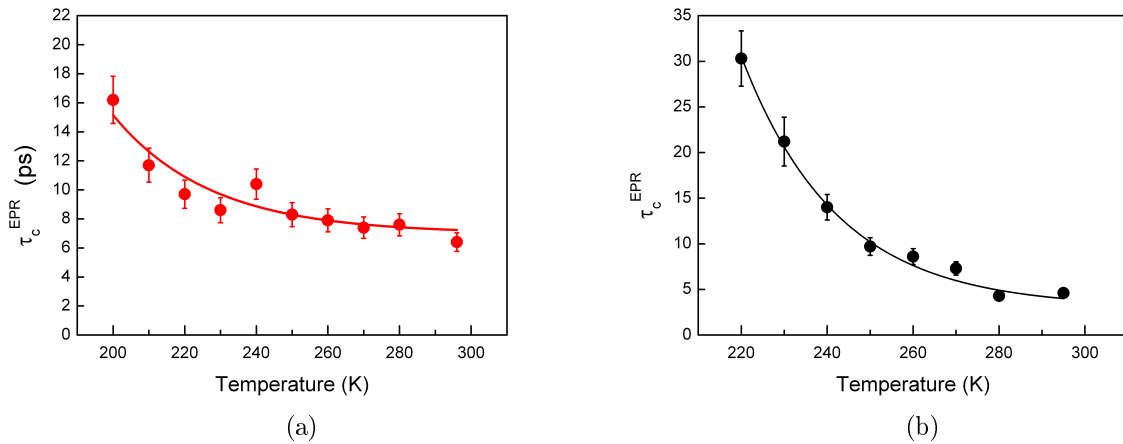


Figure S4: Correlation time of TEMPOL in (a) toluene and (b) chloroform obtained from CW-EPR measurements as a function of temperature (error bar 10%). The solid lines are the fit with the exponential function  $\tau_c^{\text{EPR}} = \tau_0^{\text{EPR}} + A \cdot \exp(-T/E)$ , where  $A$ ,  $\tau_0^{\text{EPR}}$ , and  $E$  are fit parameters.

Table S.I: Rotational correlation times from CW-EPR for different polarizing agents at room temperature (295 K). Data of fullerene-nitroxides in toluene are from Ref. [6]. Error on  $\tau_c^{\text{EPR}}$  values is  $\sim 10\%$ .

Solvent	Radical	$c$ (mM)	$\tau_c^{\text{EPR}}$ (ps)	Solvent	Radical	$c$ (mM)	$\tau_c^{\text{EPR}}$ (ps)
Toluene	TEMPOL	1	6.4	Chloroform	TEMPOL	0.5	4.6
"	TP-CLST	1.4	31.0	"	TP-CLST	0.7	48
"	FN	1.5	60	"	FN-1a	1.2	214
"	FN-1a	1.5	150	"	FN-2a	1.1	385
"	FN-2a	1.5	300	"	TEMPONE	10	4.5
"	FN-3a	1.5	450				

The diffusion constant of TEMPO in the solvent was accessed by measuring the diffusion coefficient of its reduced species TEMPONE-H (TNH, see scheme S1). We noted that TNH is not stable under ambient conditions and slowly oxidizes to its radical form, as observed via CW EPR. However, the residual  $^1\text{H}$  NMR signal of the reduced form was still readily detectable. Stability throughout the measurements of the diffusion coefficient was ensured via  $^1\text{H}$  NMR measurements. Minor impurities were detected with NMR but, as verified by cross check comparisons, they are not affecting the determination of  $D_{\text{TP},\text{s}}$ .

### S3.1 Toluene

The self diffusion coefficient of toluene  $D_{\text{tol}}$  as a function of the temperature has been previously reported by Winkelmann et al. in Ref. [35]. Those values were reproduced via PFG-NMR measurements in toluene. The temperature dependency of  $D_{\text{tol}}$  over the range 160-320 K was fitted with the Speedy-Angell function,  $D = a \cdot (T/T_0 - 1)^\gamma$  [32].

$D_{\text{TP},\text{tol}}$  was measured via PFG-NMR for TNH in deuterated toluene. Gradient strength calibration was performed by measurement of the self diffusion coefficient of  $\text{D}_2\text{O}$  (residual  $^1\text{H}$ -signal of HDO was detected) adjusting the obtained value to be  $D = 1.90 \cdot 10^{-9} \text{ m}^2/\text{s}$  [36]. Data analysis was performed as discussed in Ref. [14]. The temperature dependence of  $D_{\text{TP},\text{tol}}$  over the range 190 – 320 K was fitted using a Speedy-Angell function  $D = a \cdot (T/T_0 - 1)^\gamma$ , where, due to the limited temperature range, the parameters  $T_0$  and  $\gamma$  were obtained from  $D_{\text{tol}}$  curve.

### S3.2 Chloroform

Measurements of  $D_{\text{CHCl}_3}$  and  $D_{\text{TP},\text{CHCl}_3}$  were performed over the temperature range 218 – 310 K. Deuterated chloroform was used as solvent and the self-diffusion coefficient of  $\text{CHCl}_3$  was determined via detecting the residual  $^1\text{H}$  NMR signal. Experimental data obtained in the range 218 – 260 K shows a systematic error in the absolute value of  $D$ , probably due to convection effects [4]. Therefore, the low temperature data of  $D_{\text{CHCl}_3}$  were rescaled according to literature values at 250 K (Figure S5). The same scaling was used for  $D_{\text{TP},\text{CHCl}_3}$ . The data are reported in Table S.III. Experimental data were fitted assuming an Arrhenius like behaviour [12] (i.e.  $D(T) = a \exp(-T/T_0)$ ). The fit parameters are displayed in Table S.II.

## S4 GEOMETRY OPTIMIZATION FOR TL/TOLUENE COMPLEX

The simulation package Orca 4.0 [19] was used for geometry optimization. DFT calculations were performed at the B3LYP level of theory using the 6-311++G\*\*/G basis set. A dispersion correction as well as a continuum model accounting for dielectric properties of the solvent was used. The optimized geometries for different orientations of TEMPOL/toluene are displayed in Figure S6.

Since the electron spin density of the nitroxide is localized on the NO group (about 50% on each atom), the distances between the nearest proton of toluene and the two atoms were measured (Figure S6). The resulting average  $r_D$  was taken as the inter-spin distance. It is worth noticing that  $d$  is slightly shorter for protons of the aromatic ring ( $d = 2.7 \text{ \AA}$ ) then for the ones of the methyl group ( $d = 2.9 \text{ \AA}$ ).

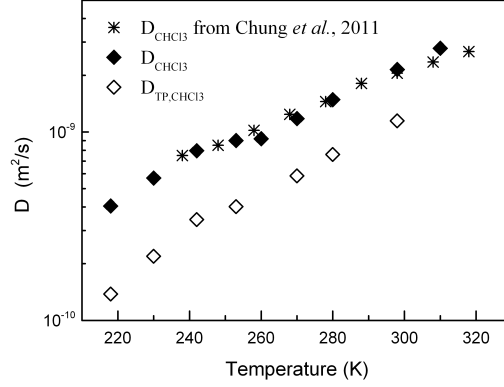


Figure S5: Diffusion coefficient of chloroform ( $D_{\text{CHCl}_3}$ ) and TNH in chloroform ( $D_{\text{TP,CHCl}_3}$ ) as a function of the temperature.

Table S.II: Parameters of the Speedy-Angell function  $D(T) = a \cdot (T/T_0 - 1)^\gamma$  used to fit  $D(T)$  of toluene in Figure 1 (main text). For chloroform experimental data were fitted to an Arrhenius function  $D(T) = a \cdot \exp(-T_0/T)$

	$a$	$T_0$	$\gamma$
$D_{\text{tol}}$	$1.49 \times 10^{-9}$	137.4	2.35
$D_{\text{TP,tol}}$	$0.72 \times 10^{-9}$	137.4	2.35
$D_{\text{CHCl}_3}$	$3.40 \times 10^{-7}$	1503	—
$D_{\text{TP,CHCl}_3}$	$3.06 \times 10^{-7}$	1671	—

Table S.III: Diffusion coefficients of TNH in toluene ( $D_{\text{TP,tol}}$ ), TNH in chloroform ( $D_{\text{TP,CHCl}_3}$ ) and self-diffusion coefficient of chloroform ( $D_{\text{CHCl}_3}$ ) as a function of the temperature. Errors are estimated to be 10% of the determined value.

Temperature (K)	$D_{\text{TP,tol}} (\times 10^{-9} \text{ m}^2/\text{s})$	$D_{\text{TP,CHCl}_3} (\times 10^{-9} \text{ m}^2/\text{s})$	$D_{\text{CHCl}_3} (\times 10^{-9} \text{ m}^2/\text{s})$
310	—	—	2.78
298	1.20	1.15	2.14
280	0.73	0.76	1.48
270	0.53	0.59	1.18
260	—	—	0.92
253	0.49	0.40	0.91
242	0.36	0.34	0.79
230	0.25	0.22	0.57
218	—	0.14	0.40

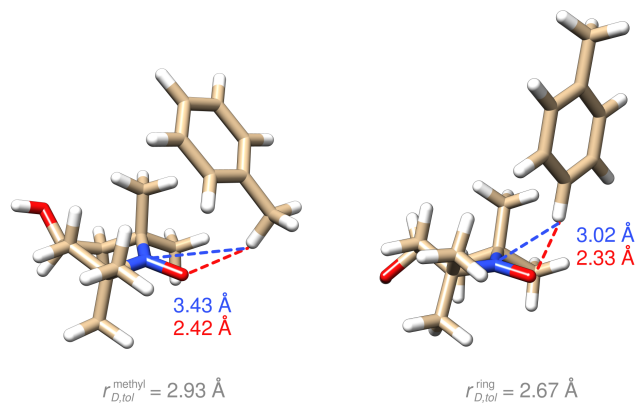


Figure S6: DFT optimized geometries for two orientations of the complex TL/toluene. Distances between the closest H atom of toluene and the two atoms on which the electron spin density is localized are marked. Color code for the structure: H - white; C - beige; N - blue; O - red.

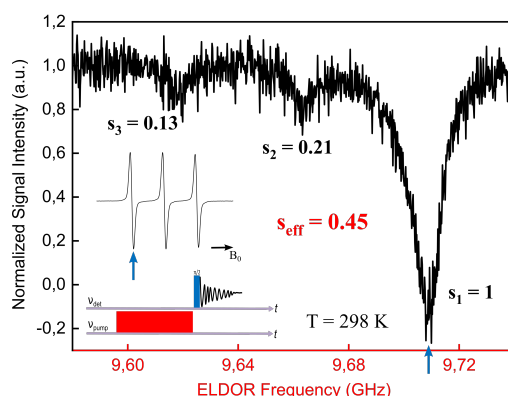


Figure S7: ELDOR curves for TEMPOL in chloroform at room temperature. The pulse sequence is displayed in the inset. Blue arrows indicate the position of the detection pulse whereas the frequency of the ELDOR pulse was swept through the EPR spectrum (red).

## S5 $^1\text{H}$ -DNP MEASUREMENTS AT 0.34 T

### S5.1 Saturation factor

The saturation factor  $s$  was obtained via ELDOR experiment [31]. In such experiment, the detection is performed on one of the EPR lines, while an ELDOR pulse ( $3 - 5 \mu\text{s}$ ) is swept in frequency through the EPR spectrum (see inset of Fig.S7). Whenever the ELDOR pulse is on resonance with an EPR line, a drop in signal intensity is observed Fig.(S7). The intensity  $s_i$  (with  $i = 1, 2, 3$ ) of these peaks depends on Heisenberg exchange and internal relaxation. The effective saturation factor is calculated by  $s_{\text{eff}} = (s_1 + s_2 + s_3)/3$ .

### S5.2 Leakage factor and $T_{\text{Build-up}}$

The leakage factor  $f$  is defined by  $f = 1 - \frac{T_{1n}}{T_{1n}^0}$ , where  $T_{1n}$  and  $T_{1n}^0$  are the nuclear relaxation times with and without polarizing agent. Nuclear relaxation times were measured using a saturation recovery experiment with FID detection (8 saturation pulses,  $\tau_{\text{sat}} = 6 \mu\text{s}$ ,  $\pi/2 = 6 \mu\text{s}$ , 60 W). Data were fitted with a single exponential function.

Additionally, the DNP build-up time  $T_{\text{Build-up}}$  was measured for each sample and temperature. The pulse sequence used consists of a MW irradiation pulse followed by an NMR detection (see Figure S8). The MW pulse duration was increased step-by-step until a steady state in signal intensity was reached. As the relaxation time is sensitive to the temperature, the comparison of  $T_{\text{Build-up}}$  measured under MW irradiation with  $T_{1n}$  measured without MW irradiation allows the evaluation of heating effects on the sample during microwave irradiation. If  $T_{\text{Build-up}} \sim T_{1n}$  holds, heating effects are negligible. Sample

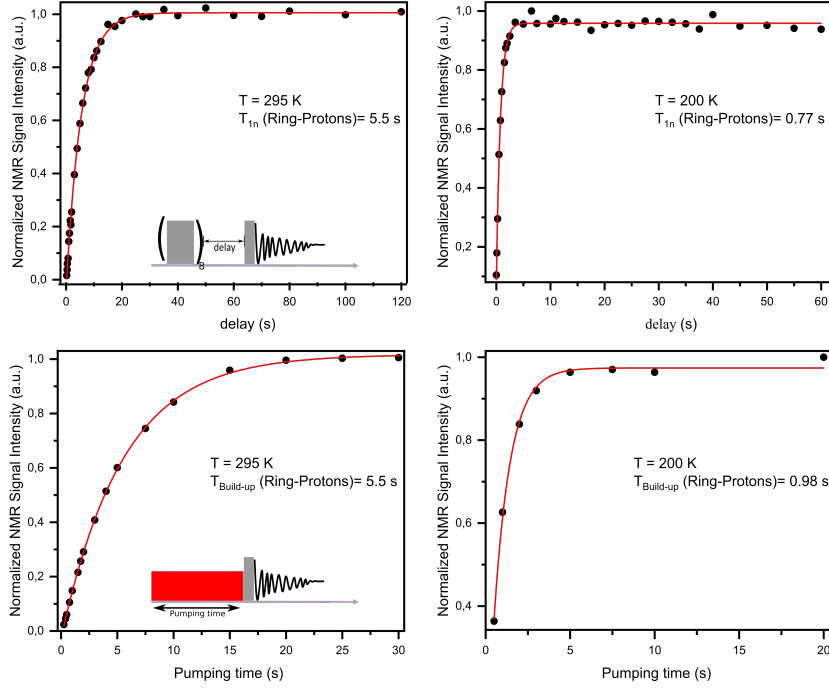


Figure S8:  $T_{1n}$  measurement (top) and  $T_{\text{Build-up}}$  measurement (bottom) obtained at two representative temperatures for a sample of toluene (aromatic ring protons) doped with TEMPOL. Red curves represent exponential fits.

heating is negligible for toluene except the two lowest temperatures (Table S.IV) while it is not for chloroform (Table S.V). Consequently, the build-up time has been used as a calibration for the local temperature of the sample under MW irradiation. According to this, the obtained coupling factors have been adjusted to their respective local sample temperature.

### S5.3 NMR enhancement

DNP enhancements were evaluated by comparing the NMR intensities recorded with (DNP) and without (Boltzmann) microwave irradiation. Boltzmann signals were acquired with a number of scans  $n_{\text{Bltz}} = 4 - 128$  and a recycle delay of  $5 \cdot T_{1n}$ . DNP signals were obtained after a MW pulse lasting several seconds. Two example spectra are shown in Figure S9. The maximum enhancement was obtained by irradiating with MW for a pumping time  $\sim 5 \cdot T_{\text{Build-up}}$ . The enhancements  $\epsilon$  were then evaluated considering the signal integrals  $I$ :

$$\epsilon = \frac{I_{\text{DNP}}}{I_{\text{Bltz}}} \cdot \frac{n_{\text{Bltz}}}{n_{\text{DNP}}} \quad (\text{S1})$$

## S6 $^1\text{H}$ -COUPLING FACTOR $\xi_{1\text{H}}$

### S6.1 Experimental data

The coupling factor  $\xi$  was obtained with the Overhauser equation  $\xi = (\epsilon - 1) / \left( s_{\text{eff}} f \frac{\gamma_e}{\gamma_n} \right)$ , where  $s_{\text{eff}}$ ,  $f$ , and  $\epsilon$  were experimentally measured as described in the previous sections. Table S.IV and S.V summarize the Overhauser parameters for TEMPOL in toluene and chloroform, respectively, obtained at 0.34 T. Table S.VI reports the coupling factor measured at 0.34 T and room temperature for nitroxide derivatives. The nitroxide derivative TP-CLST was not tested in toluene due to an anomalous broadening of the NMR line, which was ascribed to radical/solvent aggregation. The influence of radical concentration  $c$  was tested in chloroform doped with 10 mM of TEMPOL and FN-2a, revealing that, within this range,  $c$  does not affect  $\xi$ . These results are summarized in Table S.VII.

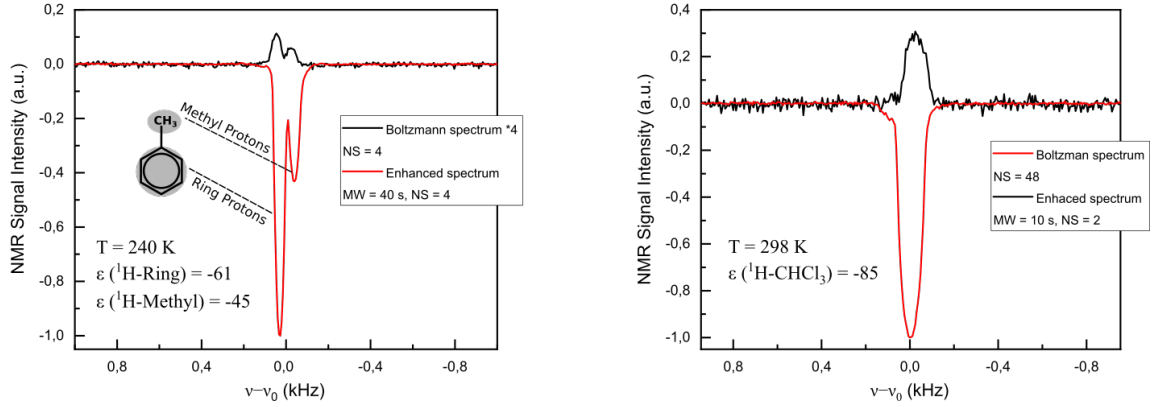


Figure S9:  $^1\text{H}$ -DNP spectra at 0.34 T of toluene (left) and chloroform (right) doped with TP. The chemical shift difference between enhanced and thermal equilibrium spectra is due to field instabilities during the measurements time, since the magnet was not equipped with locking.

Table S.IV: Nuclear relaxation times and Overhauser parameters for each temperature measured in toluene at 0.34 T. The sample was doped with  $\sim 1\text{--}1.5$  mM of TEMPOL. Protons belonging to the aromatic ring and the methyl group are distinguished. Error on  $f$  and  $s_{\text{eff}}$  is  $\sim 5\%$ , while for  $\epsilon$  is  $\sim 10\%$ . Error on  $\xi$  has been quantified as 15%.

Aromatic ring protons							
Temperature (K)	$T_{1,n}$ (s)	$T_{\text{Build-up}}$ (s)	$T_{1,n}^{\text{dia}}$ (s) <sup>a</sup>	$f$	$s_{\text{eff}}$	$\epsilon$	$\xi$
210 <sup>b</sup>	1.1	1.0	1.9	0.52	0.63	-13.3	0.057
220 <sup>b</sup>	1.5	1.55	2.3	0.52	0.60	-22.4	0.11
220	1.5	1.63	3.3	0.54	0.60	-28.2	0.14
230	1.9	2.0	4.5	0.57	0.57	-33.5	0.16
240	2.6	2.4	5.3	0.52	0.59	-33.8	0.17
250	2.8	2.8	7.1	0.61	0.55	-43.3	0.20
260	3.2	3.4	8.2	0.60	0.57	-59.5	0.26
270	4.0	3.9	10.5	0.62	0.59	-59.8	0.25
280	4.5	4.1	11.4	0.61	0.51	-55.8	0.28
297	5.5	5.5	12.5	0.56	0.58	-61.1	0.29

Methyl group protons							
Temperature (K)	$T_{1,n}$ (s)	$T_{\text{Build-up}}$ (s)	$T_{1,n}^{\text{dia}}$ (s)	$f$	$s_{\text{eff}}$	$\epsilon$	$\xi$
210 <sup>b</sup>	1.1	1.1	1.5	0.45	0.63	-8.8	0.052
220 <sup>b</sup>	1.8	1.8	2.0	0.38	0.60	-15.5	0.11
220	1.8	1.7	2.9	0.38	0.60	-18.8	0.12
230	1.9	2.0	3.7	0.49	0.57	-24.3	0.13
240	2.2	2.2	4.3	0.49	0.59	-31.6	0.16
250	2.4	2.6	5.3	0.55	0.55	-31.7	0.15
260	3.3	3.1	6.3	0.48	0.57	-35.0	0.19
270	3.7	3.8	7.1	0.48	0.59	-36.7	0.25
280	4.1	3.6	7.5	0.45	0.51	-44.7	0.29
297	4.7	4.7	8.1	0.42	0.58	-44.8	0.28

<sup>a</sup>  $T_{1,n}$  of toluene without radical. <sup>b</sup> Temperature calibrated with  $T_{\text{Build-up}}$ .



Table S.V: Nuclear relaxation times and Overhauser parameters for each temperature measured in chloroform at 0.34 T. The sample was doped with  $\sim 0.5\text{--}1$  mM of TEMPOL. For repeated measurements, the average of the coupling factor values has been reported in the main text. Errors on  $f$  is  $\sim 5\%$ , while for  $\epsilon$  and  $s_{\text{eff}}$  is  $\sim 10\%$ . Error on  $\xi$  has been quantified as  $15\%$ .

Temperature (K)	$T_{1,n}$ (s)	$T_{\text{Build-up}}$ (s)	$T_{1,n}^{\text{dia}}$ (s) <sup>a</sup>	$f$	$s_{\text{eff}}$	$\epsilon$	$\xi$
230 <sup>b</sup>	1.1	1.15	29.3	0.96	0.63	-24	0.063
230 <sup>b</sup>	1.1	1.15	29.3	0.97	0.61	-43	0.11
240 <sup>b</sup>	1.55	1.4	32.8	0.96	0.39	-36	0.15
240 <sup>b</sup>	1.55	1.4	32.8	0.96	0.55	-44	0.13
250 <sup>b</sup>	1.69	1.8	38.1	0.96	0.46	-55	0.19
250 <sup>b</sup>	1.69	1.8	38.1	0.96	0.50	-58	0.18
250	1.69	1.8	44.9	0.96	0.48	-49	0.16
250	1.69	1.8	44.9	0.96	0.48	-55	0.18
260	2.1	2.1	52.7	0.96	0.45	-57	0.20
270	2.2	2.3	61.2	0.96	0.49	-60	0.19
270	2.2	2.3	61.2	0.96	0.45	-55	0.19
280 <sup>c</sup>	2.7	2.4	69.9	0.96	0.44	-62	0.22
280 <sup>c</sup>	—	—	69.9	$\approx 0.96$	0.45	-81	0.28
297	2.8	2.9	82.5	0.97	0.45	-85	0.30 <sup>d</sup>

<sup>a</sup>  $T_{1,n}$  of chloroform without radical. <sup>b</sup> Temperature calibrated with  $T_{\text{Build-up}}$ . <sup>c</sup> Due to temperature instabilities, error on this data point has been quantified as  $20\%$ . <sup>d</sup> Within the experimental error, the value agrees with the prediction from MD theory reported in Ref. [16].

Table S.VI: Nuclear relaxation times and Overhauser parameters for chloroform doped with nitroxide derivatives ( $c \sim 1\text{--}1.5$  mM) at room temperature at 0.34 T.

Solvent	Radical	$T_{1,n}$ (s)	$T_{\text{Build-up}}$ (s)	$f$	$s_{\text{eff}}$	$\epsilon$	$\xi$
Chloroform	TP-CLST	2.2	2.2	0.97	0.60	-104	0.27
Chloroform	FN-1a	0.9	0.9	0.99	0.86	-104	0.21
Chloroform	FN-2a	0.7	0.7	0.99	0.87	-116	0.20

Table S.VII: Nuclear relaxation times and Overhauser parameters at 0.34 T for TEMPOL and FN-2a in chloroform at room temperature. Radical concentration was  $\sim 10$  mM.

Solvent	Radical	$T_{1,n}$ (s)	$T_{\text{Build-up}}$ (s)	$f$	$s_{\text{eff}}$	$\epsilon$	$\xi$
Chloroform	TEMPOL	0.18	0.13	0.998	0.70	-170	0.37 <sup>a</sup>
Chloroform	FN-2a	0.11	0.10	0.998	0.93	-121	0.20

<sup>a</sup> A severe temperature deviation has been observed for this sample, causing a shift of the coupling factor value with respect to the one measured with  $c \sim 1$  mM (Table S.V).

Table S.VIII: Nuclear relaxation times and  $^{13}\text{C}$  Overhauser parameters for nitroxide derivatives at room temperature at 1.2 T. Radical concentration is  $\approx 10$  mM for all the samples. Relative error in coupling factors is 15%.

Solvent	Radical	$T_{1,n}$ (s)	$T_{\text{Build-up}}$ (s)	$f$	$s_{\text{eff}}$	$\epsilon$	$\xi$
$^{13}\text{CCl}_4$	TN	18.5	16.6	0.925	0.25	252	$-0.41^{\text{a}}$
$^{13}\text{CCl}_4$	TP-CLST	2.9	3.4	0.99	0.12	150	$-0.48$
$^{13}\text{CCl}_4$	FN-2a	19.6	18.4	0.90	0.28	425	$-0.64$
$^{13}\text{CCl}_4$	FN-2a	3.8	3.8	0.98	0.33	550	$-0.65^{\text{a}}$
$^{13}\text{CHCl}_3$	TN	4.5	4.0	0.85	0.25	260	$-0.46^{\text{a}}$
$^{13}\text{CHCl}_3$	TP-CLST	2.8	2.9	0.90	0.29	350	$-0.51$
$^{13}\text{CHCl}_3$	FN1a	2.6	2.8	0.92	0.22	355	$-0.67^{\text{b}}$
$^{13}\text{CHCl}_3$	FN-2a	3.5	3.1	0.89	0.30	370	$-0.53^{\text{a}}$

<sup>a</sup> Ref. [22]. <sup>b</sup> Instability of the fullerene nitroxide FN-1a was observed in labelled compound  $^{13}\text{C}$  labelled chloroform. Error for this data point has been estimated as 20%.

## S7 $^{13}\text{C}$ -DNP MEASUREMENTS

$^{13}\text{C}$ -DNP experiments at 1.2 T were performed on an instrument having both EPR and NMR capabilities, and whose technical details have been described elsewhere [22]. A custom made copper coil was inserted in a Bruker cylindrical resonator (ER-5106QT/W) to enable NMR detection. Samples (5-8  $\mu\text{L}$ ) were filled in quartz tube with a 1.6 mm outer diameter, and then degassed with freeze-pump-thaw cycles. The effective saturation factor  $s_{\text{eff}}$  was measured with ELDOR sequence, as described in Section S5. Due to the lack of NMR sensitivity, the nuclear relaxation time  $T_{1,n}$  was measured recording the signal intensity as a function of the delay time after a MW pump pulse. The latter was calibrated to observe the  $^{13}\text{C}$  NMR signal and limit heating effects. Overhauser parameters obtained at 1.2 T are summarised in Table S.VIII.

$^{13}\text{C}$  enhancements at 9.4 T and 14.1 T have been previously published in Ref. [22]. The effective saturation  $s_{\text{eff}}$  at 14.1 T was previously estimated as  $s_{\text{eff}} \sim 0.1$  and, being  $f \sim 0.98$  for  $c \sim 10$  mM, the coupling factor results  $\xi_{^{13}\text{C}} = -0.01$ . The effective saturation could not be experimentally measured at 9.4 T. We assumed a variability interval between  $s_{\text{eff}} = 0.1$ , considering that the MW is provided by a gyrotron source [22], and  $s_{\text{eff}} = 0.6$ , which can be assumed as the maximum value in case the irradiated line is fully saturated [6]. Therefore, the coupling factor range is  $\xi_{^{13}\text{C}} = 0.0002 - 0.035$ . Despite the error is quite large, the absolute values are small and do not compromise our analysis.

## S8 RELAXATION MODEL FOR $\xi$

Within the Overhauser DNP theory, the relaxation model as described in Ref. [2, 23, 26] predicts the coupling factor  $\xi$  as:

$$\xi = \frac{5}{7} \left( 1 - \frac{3k_{\text{D}}J_{\text{D}}(\omega_{\text{n}}, \tau_{\text{D}}) + 3k_{\text{rot}}J_{\text{rot}}(\omega_{\text{n}}, \tau_{\text{c}})}{R_{1,\text{D}} + R_{1,\text{rot}} + R_{1,\text{cont}}} \right) - \frac{12}{7} \left( \frac{R_{1,\text{cont}}}{R_{1,\text{D}} + R_{1,\text{rot}} + R_{1,\text{cont}}} \right) \quad (\text{S2})$$

where  $R_1$  are the nuclear relaxation rates for translational diffusion ( $R_{1,\text{D}}$ ), rotation ( $R_{1,\text{rot}}$ ) and contact ( $R_{1,\text{cont}}$ ) contributions.

The relative translational diffusion between the two species is described by the force-free hard-sphere model (ffHS), where the spins  $I$  and  $S$  are considered at the centre of the two respective spherical molecules [13, 24]. The spectral density is:

$$J_{\text{D}}(\omega_i, \tau_{\text{D}}) = \frac{1 + 5z/8 + z^2/8}{1 + z + z^2/2 + z^3/6 + 4z^4/81 + z^5/81 + z^6/648} \quad (\text{S3})$$

where  $z = \sqrt{2\omega_i\tau_D}$ , with  $\tau_D$  being the correlation time and  $\omega_e(\omega_n)$  is the electron(nuclear) Larmor frequency.  $\tau_D$  is defined as  $\tau_D = r_D^2/(D_s + D_{r,s})$ , where  $r_D$  is the distance of minimum approach, while  $D_s$  and  $D_{r,s}$  are the self diffusion coefficient of the solvent and the one of the radical in the solvent, respectively. The corresponding nuclear relaxation rate is:

$$R_{1,D} = k_D [7J_D(\omega_e, \tau_D) + 3J_D(\omega_n, \tau_D)] \quad (S4)$$

with

$$k_D = \frac{32000\pi}{405} \left(\frac{\mu_0}{4\pi}\right)^2 \frac{N_A c \gamma_n^2 g_e^2 \mu_B^2 S(S+1)}{r_D(D_s + D_{r,s})} \quad (S5)$$

where  $N_A$  is the Avogadro number;  $c$  is the concentration of polarizing agent;  $\gamma_n$  is the gyromagnetic ratio in rad·Hz/T;  $g_e$  is the electron Landé factor;  $\mu_0$  is the permeability constant and  $\mu_B$  is the Bohr magneton.

A second dipole-dipole interaction arising from solvent molecules bound to the paramagnetic agent [26], or from “spin eccentricity” effects [15, 23], can be included with a Lorentzian contribution as phenomenological expression [26]. Hereby, we use the same approach to introduce a dipolar contribution modulated with the rotational correlation time of the polarizing agent. The spectral density and the corresponding nuclear relaxation rate are:

$$J_{\text{rot}}(\omega, \tau_c) = \frac{\tau_c}{1 + \omega^2 \tau_c^2} \quad (S6)$$

$$R_{1,\text{rot}} = k_{\text{rot}} [7J_{\text{rot}}(\omega_e, \tau_c) + 3J_{\text{rot}}(\omega_n, \tau_c)] \quad (S7)$$

where  $\tau_c$  is the rotational correlation time and  $k_{\text{rot}}$  is the amplitude.

Finally, a scalar contribution arising from the modulation of the Fermi contact interaction between the two species has to be considered. The Pulse model describes collisions between polarizing agent and solvent molecule having a duration  $\tau_i$  and a collision frequency  $1/\tau_{p,i}$ . The associated spectral density is:

$$J_{\text{cont}}(\omega_e, \tau_i) = \sum_i \frac{\langle A_i \rangle^2}{\hbar^2 \tau_{p,i}} [\tau_i \cdot \exp(-\tau_i \omega_e)]^2 \quad (S8)$$

where the index  $i$  characterizes each type of contact and  $A_i$  is the hyperfine coupling. The nuclear relaxation rate is:

$$R_{1,\text{cont}} = \frac{2}{3} S(S+1) J_{\text{cont}}(\omega_e, \tau_i) \quad (S9)$$

## S9 SIMULATIONS OF $\xi_{1H}$

The fit of  $\xi_{1H}$  as a function of the temperature for TP either in chloroform or toluene was performed with Eq. S2. The rotational contribution  $R_{1,\text{rot}}$  and the scalar component  $R_{1,\text{cont}}$  are both negligible, as described in the main text. Therefore, Eq. S2 reduces to:

$$\xi = \frac{5}{7} \left( 1 - \frac{3J_D(\omega_n, \tau_D)}{7J_D(\omega_e, \tau_D) + 3J_D(\omega_n, \tau_D)} \right) \quad (S10)$$

where  $J_D(\omega_i, \tau_D)$  is defined by the ffHS model (Eq. S3). The diffusion coefficients  $D_s$  and  $D_{TP,s}$  have been obtained as described in Section S3. Consequently, the fit required only  $r_D$  as fit parameter. The best fit is obtained for  $r_D^{\text{ring}} = 3.5 \text{ \AA}$  and  $r_D^{\text{methyl}} = 3.9 \text{ \AA}$  for toluene, and  $r_D = 3.65 \text{ \AA}$  for chloroform.

$\xi_{1H}$  for nitroxide derivatives as polarizing agents was measured at room temperature and simulated with Eq. S2 as a function of the rotational correlation time  $\tau_c = \tau_c^{\text{EPR}}$ . With the scalar contribution being  $R_{1,\text{cont}} = 0$ , Eq. S2 results:

$$\xi = \frac{5}{7} \left( 1 - \frac{3k_{\text{rot}} J_{\text{rot}}(\omega_n, \tau_c) + 3k_D J_D(\omega_n, \tau_D)}{R_{1,D} + R_{1,\text{rot}}} \right) \quad (S11)$$

The translational diffusion contribution is completely defined (i.e.  $R_{1,D}$  independent of  $\tau_c^{\text{EPR}}$ ) by the diffusion coefficient  $D_s$  (for either chloroform or toluene), the distance of minimum approach  $r_D$  as

Table S.IX: Fit parameters used in Equation S11 to fit  $\xi_{1H}$  as a function of the correlation time  $\tau_c = \tau_c^{\text{EPR}}$ . Error on  $k_{\text{rot}}$  is  $\sim 10\%$ .

Solvent	$D_s$ (m <sup>2</sup> /s) <sup>a</sup>	Translational diffusion		$c$ (mM)	Rotation $k_{\text{rot}}$
		$r_D$ (Å)	$\tau_D$ (ps) <sup>b</sup>		
Toluene (ring)	$2.14 \times 10^{-9}$	3.5	57	1.5	$0.8 \times 10^8$
Toluene (methyl)	$2.14 \times 10^{-9}$	3.9	73	1.5	$0.8 \times 10^8$
Chloroform	$2.16 \times 10^{-9}$	3.65	61	1	$0.5 \times 10^8$

<sup>a</sup> Self-diffusion coefficient of the solvent at 297 K. <sup>b</sup>  $\tau_D = r_D^2/D_s$ .

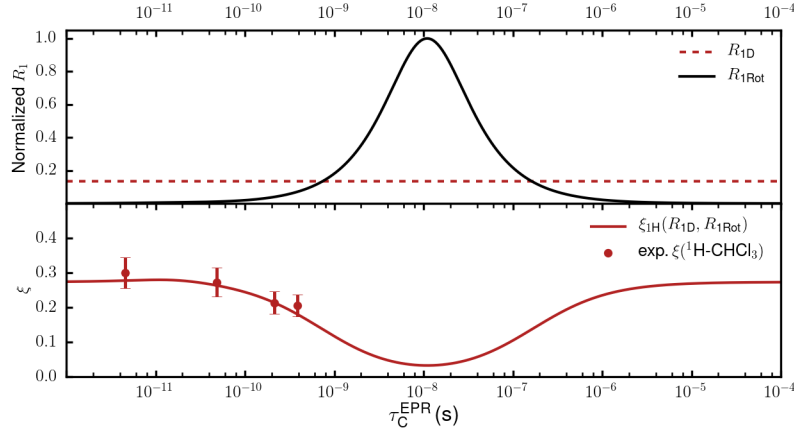


Figure S10: Experimental data (red dots) and simulation (red line) of  $\xi_{1H}$  as a function of  $\tau_c$  of the PA in  $\text{CHCl}_3$ .  $R_{1,\text{rot}}$  (black line) and  $R_{1,D}$  (dashed red) are displayed in the top panel. For clarity, values were normalized to unity as a maximum value.

determined from the previous analysis, and the radical concentration  $c$  experimentally determined. The rotational contribution has  $\tau_c = \tau_c^{\text{EPR}}$  as correlation time, where  $\tau_c^{\text{EPR}}$  was measured by CW-EPR (Section S2). The amplitude  $k_{\text{rot}}$  is the only fit parameter, and resulted  $k_{\text{rot}} = 0.8 \times 10^8$  for toluene and  $k_{\text{rot}} = 0.5 \cdot 10^8$  for chloroform. The summary of the parameters used in the fit procedure is reported in Table S.IX.

Figure S10 is the same figure as Figure 2 in the main text with a larger  $\tau_c^{\text{EPR}}$  range. It showcases that for very short and very long  $\tau_c^{\text{EPR}}$  values ( $20 \times 10^{-12} \text{ s} > \tau_c > 10^{-5} \text{ s}$ ),  $R_{1,\text{rot}}$  becomes negligible and the coupling factor is dominated by translational diffusion.

## S10 SIMULATIONS OF $\xi_{13C}$

Coupling factor  $\xi_{13C}$  was measured at room temperature in  $^{13}\text{CCl}_4$  and  $^{13}\text{CHCl}_3$  doped with nitroxide derivatives. Eq. S2 can be used to predict  $\xi_{13C}$  as a function of  $\tau_c$ . The translational diffusion contribution was computed with the ffHS model and the values  $r_D$  from Ref. [22] and the diffusion coefficient rescaled for large polarizing agent, as described in the main text. We note that  $r_D$  is larger for  $^{13}\text{C}$  (3.85 Å) than for  $^1\text{H}$  (3.65 Å), as expected. However, as previously noted by Sezer in Ref. [28],  $r_D$  only partly correlate with a single structural property, while it reflects a more complex dynamic behaviour (and includes, for instance, the angle of approach). Therefore, the comparison of  $r_D$  extracted from the ffHS model should take into account such approximation.

The contact contribution was described with the Pulse model (Eq. S8) and consists of short timescale collisions with duration  $\tau_1 = 0.5$  ps [17,22]. The rotational contribution was calculated with: (i) the amplitude  $k_{\text{rot}}$  obtained from the analysis performed at 0.34 T and rescaled linearly for a concentration

Table S.X: Parameters used for simulating  $\xi_{13\text{C}}$  as a function of  $\tau_c$  at 1.2 T for  $^{13}\text{CCl}_4$  (Eq. S12) and  $^{13}\text{CHCl}_3$  (Eq. S13) doped with nitroxide derivatives.

	Translational diffusion <sup>a</sup>	Rotation	Contact 1 <sup>a</sup>			Contact 1,H <sup>a</sup>	
	$\tau_D$	$k_{\text{rot}}$	$\tau_c^{\text{EPR}}$	$\sqrt{F_1}$	$\tau_1$	$\sqrt{F_{1,H}}$	$\tau_{1,H}$
$\text{CCl}_4$	115 ps <sup>b</sup>	$5 \cdot 10^8$	637 ps	$1.25 \cdot 10^{12}$ rad/s	0.5 ps	—	—
$\text{CHCl}_3$	76/55 ps <sup>c</sup>	$5 \cdot 10^8$	385 ps	$1.25 \cdot 10^{12}$ rad/s	0.5 ps	$0.5 \cdot 10^{12}$ rad/s	12 ps

<sup>a</sup> Ref. [22]. <sup>b</sup>  $r_D^{\text{Cl}} = 4.0 \text{ \AA}$ ;  $D_{\text{CCl}_4} = 1.4 \cdot 10^{-9} \text{ m}^2/\text{s}$ . <sup>c</sup>  $r_D^{\text{Cl}} = 4.0 \text{ \AA}$ ;  $r_D^{\text{H}} = 3.4 \text{ \AA}$ ;  $D_{\text{CHCl}_3} = 2.1 \cdot 10^{-9} \text{ m}^2/\text{s}$ .

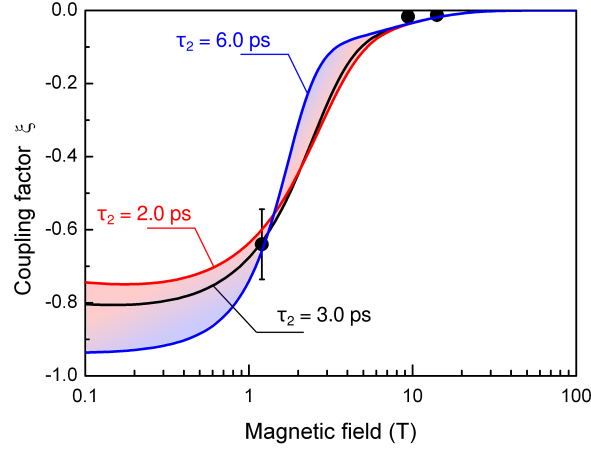


Figure S11: Coupling factor of FN-2a in  $\text{CCl}_4$  as a function of the magnetic field. The simulations were performed with Eq. S12 and a second contact contribution  $R_{1,\text{cont}2}$  with  $\tau_2$  as collision time and  $\sqrt{F_2} = 1.2 \cdot 10^{12}$  as amplitude.

of  $c \sim 10 \text{ mM}$ ; since a bound state due to secondary interactions is unlikely, we did not include other scaling factors (such as the distance). (ii)  $\tau_c = \tau_c^{\text{EPR}}$ , where  $\tau_c^{\text{EPR}}$  was measured by CW-EPR for FN-2a. For  $^{13}\text{CCl}_4$  doped with nitroxide derivative, the coupling factor results:

$$\xi = \frac{5}{7} \left( 1 - \frac{3k_D^{\text{Cl}} J_D(\omega_n, \tau_D^{\text{Cl}}) + 3k_{\text{rot}} J_{\text{rot}}(\omega_n, \tau_c)}{R_{1,D}^{\text{Cl}} + R_{1,\text{rot}} + R_{1,\text{cont}1}} \right) - \frac{12}{7} \left( \frac{R_{1,\text{cont}}}{R_{1,D}^{\text{Cl}} + R_{1,\text{rot}} + R_{1,\text{cont}1}} \right) \quad (\text{S12})$$

In the case of chloroform, the polarization transfer is mediated by either H or Cl. The coupling factor has been calculated considering 3/4 of the  $\text{CCl}_4$  contribution, accounting for Cl mediated collisions and diffusion [17, 22]:

$$\xi = \frac{5}{7} \left( 1 - \frac{0.75 \cdot 3k_D^{\text{Cl}} J_D^{\text{Cl}}(\omega_n, \tau_D^{\text{Cl}}) + 3k_D^{\text{H}} J_D^{\text{H}}(\omega_n, \tau_D^{\text{H}}) + 3k_{\text{rot}} J_{\text{rot}}(\omega_n, \tau_c)}{0.75 \cdot R_1^{\text{Cl}} + R_{1,\text{rot}} + R_{1,D}^{\text{H}} + R_{1,\text{cont}1,\text{H}}} \right) - \frac{12}{7} \left( \frac{0.75 \cdot R_{1,\text{cont}1} + R_{1,\text{cont}1,\text{H}}}{0.75 \cdot R_1^{\text{Cl}} + R_{1,\text{rot}} + R_{1,\text{cont}1,\text{H}}} \right) \quad (\text{S13})$$

where  $R_1^{\text{Cl}} = R_{1,D}^{\text{Cl}} + R_{1,\text{cont}1}$ . Table S.X shows a summary of the parameters used for simulating  $\xi_{13\text{C}}$  at 1.2 T as a function of  $\tau_c$  for  $^{13}\text{CCl}_4$  and  $^{13}\text{CHCl}_3$ .

The field dependence of  $\xi_{13\text{C}}$  was investigated for  $^{13}\text{CCl}_4$  and  $^{13}\text{CHCl}_3$  doped with FN-2a. The coupling factor was simulated with Eq. S12 and Eq. S13 plus an additional contact component  $R_{1,\text{cont}2}$  described with the Pulse model and having  $\sqrt{F_2} = 1.2 \cdot 10^{12}$  for  $\text{CCl}_4$  ( $\sqrt{F_2} = 0.8 \cdot 10^{12}$  for  $\text{CHCl}_3$ ) and  $\tau_2 = 3.0 \text{ ps}$  (see Table 2 in the main text). The latter has been chosen as the best fit parameter within the range  $\tau_2 = 2.0 - 6.0 \text{ ps}$  (Figure S11).

## S11 DFT AND MD SIMULATIONS OF TEMPONE AND FN-2a

### S11.1 DFT calculations

All calculations were performed with Orca 4.0.1 [19,20]. For the investigation of the conformations of the TN and FN-2a polarizing agents, geometry optimizations were performed using the B3LYP functional in combination with the def2-TZVPP basis set [34]. Additionally, the resolution-of-the-identity and chains-of-spheres approximations (RIJCOSX with def2/J auxiliary basis set) as well as dispersion correction (D3BJ) were employed [9, 10, 21, 33]. Tight convergence criteria for the SCF (TIGHTSCF) and the optimization procedure (TIGHTOPT) were chosen. For comparison of the relative energies of the various conformations, the calculated dispersion corrections were neglected. To reduce the computational demand, a small model system for FN-2a was used, wherein only two six-membered rings of the C<sub>60</sub> moiety were retained. Graphical representations of the determined minima and corresponding relative energies are summarized in Figures S12 and S13.

### S11.2 MD parameters and simulations

#### S11.2.1 Partial charges

Partial charges for chloroform and TN were obtained by the following approach: the structure of the respective system was geometry-optimized (Orca 4.0.1, HF/6-31g\*). Based on this, charges were fitted using the RESP methodology as implemented in Multiwfn 3.6 [1, 18]. During the fitting procedure, identical charges were imposed for symmetry-related positions. Charges for chemically equivalent groups (e.g. nitroxide methyl groups) were subsequently averaged. The charges for chloroform are summarized in Table S.XI. Notably, the values for Cl and H are close to previously reported data with some variation for the central carbon atom [8].

The large system size of FN-2a leads to uneconomical computational demand of the direct DFT investigation. In addition, the RESP methodology is known to give inaccurate results for buried atoms [1]. Thus, charges for this molecule were determined using several smaller models for parts of the system. The structures of all model systems were geometry-optimized (Orca 4.0.1, HF/6-31g\*), prior to RESP fitting. First, the effect of the radical linker on the fullerene was investigated using a system containing a C<sub>60</sub> core and an attached *N*-methyl pyrrolidine ring (see Figure S16, left). RESP fitting showed that all fullerene carbon atoms except those in the pyrrolidine ring (+0.40319 e) have charges very close to zero with a total charge of -0.34694 e (sum over 58 atoms).

Similarly, a model of a fullerene with an attached dimethyl malonate ester was used to study the effect of this type of substitution (Figure S16, right). For this second system, RESP fitting indicated that the fullerene carbons in the cyclopropane ring (+0.54709 e) and their nearest neighbors (-0.19764 e) have partial charges significantly different from zero, leaving a total of +0.20118 e on the remaining 52 fullerene carbon atoms. The charges for the malonate group were also derived on this model and is included in Table S.XIII. Finally, the sum charge of the methyl groups (0.50406 e) was used as a restraint for the charges of the various chain conformations (see below).

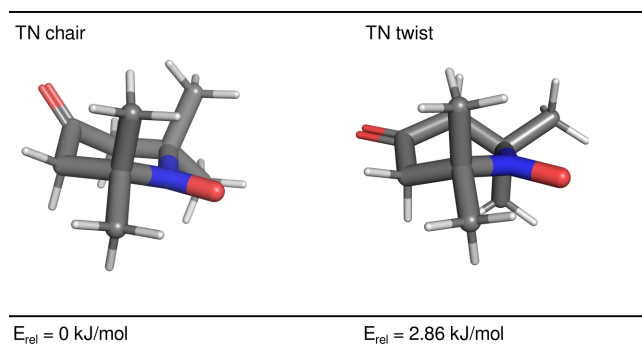


Figure S12: DFT-optimized conformations and relative energies (excluding dispersion correction) for TEMPONE.

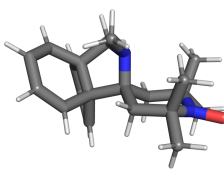
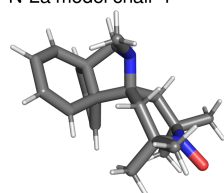
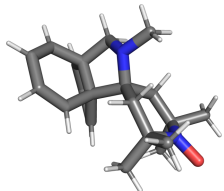
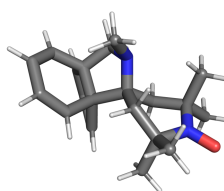
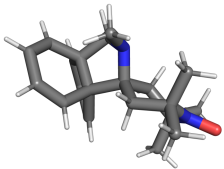
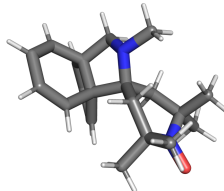
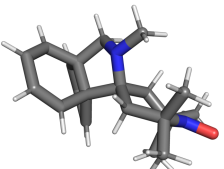
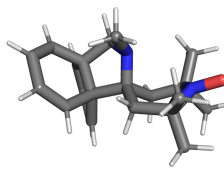
FN-2a model chair-1	FN-2a model chair-1
	
$E_{\text{rel}} = 0 \text{ kJ/mol}$	$E_{\text{rel}} = 34.42 \text{ kJ/mol}$
FN-2a model chair-3	FN-2a model twist-1
	
$E_{\text{rel}} = 28.82 \text{ kJ/mol}$	$E_{\text{rel}} = 11.48 \text{ kJ/mol}$
FN-2a model twist-2	FN-2a model twist-3
	
$E_{\text{rel}} = 8.42 \text{ kJ/mol}$	$E_{\text{rel}} = 20.43 \text{ kJ/mol}$
FN-2a model twist-4	FN-2a model boat
	
$E_{\text{rel}} = 24.23 \text{ kJ/mol}$	$E_{\text{rel}} = 4.35 \text{ kJ/mol}$

Figure S13: DFT-optimized conformations and relative energies (excluding dispersion correction) for the FN-2a model system.

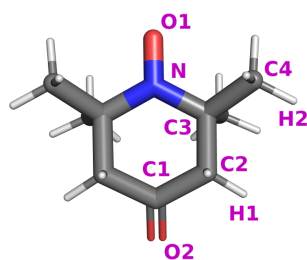


Figure S14: Atom numbering scheme for TEMPONE.

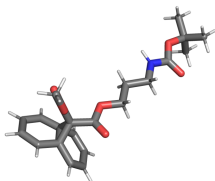
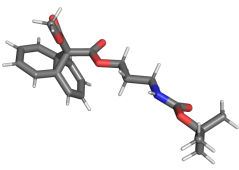
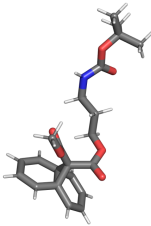
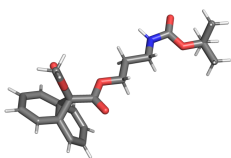
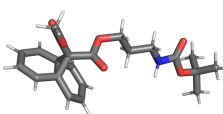
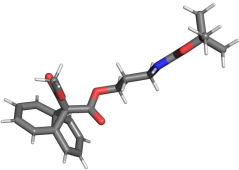
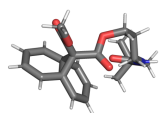
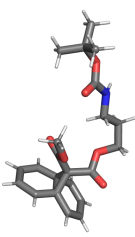
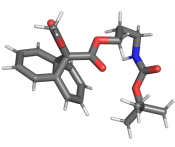
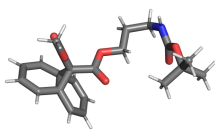
chain model configuration 1	chain model configuration 2	chain model configuration 3
		
$E_{\text{rel}} = 0 \text{ kJ/mol}$	$E_{\text{rel}} = 4.35 \text{ kJ/mol}$	$E_{\text{rel}} = 44.76 \text{ kJ/mol}$
chain model configuration 4	chain model configuration 5	chain model configuration 6
		
$E_{\text{rel}} = 6.54 \text{ kJ/mol}$	$E_{\text{rel}} = 3.75 \text{ kJ/mol}$	$E_{\text{rel}} = 2.13 \text{ kJ/mol}$
chain model configuration 7	chain model configuration 8	chain model configuration 9
		
$E_{\text{rel}} = 6.42 \text{ kJ/mol}$	$E_{\text{rel}} = 3.10 \text{ kJ/mol}$	$E_{\text{rel}} = 26.19 \text{ kJ/mol}$
chain model configuration 10		
		
$E_{\text{rel}} = 7.50 \text{ kJ/mol}$		

Figure S15: DFT-optimized conformations and relative energies (excluding dispersion corrections) for the chain model system.

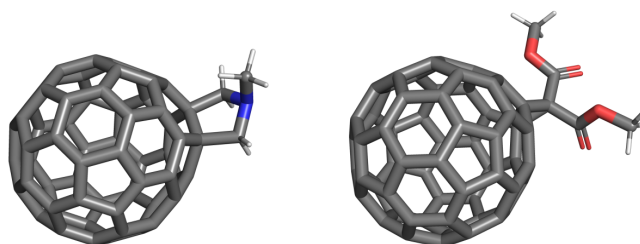


Figure S16: Model systems for investigations of fullerene charges.



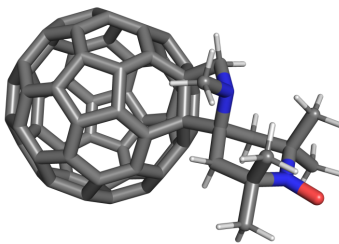


Figure S17: Model system for the determination of the partial charges of the nitroxide group and linker.

Next, the charges of the TEMPO radical and pyrrolidine linker were inferred from the model depicted in Figure S17, corresponding to the most favorable conformation as determined by DFT (chair-1, see above). For the RESP fitting procedure, the charges of the fullerene carbon atoms were fixed to  $+0.40319$  e for those in the pyrrolidine ring and  $-0.00598$  e for the remainder ( $-0.34694$  e evenly distributed over 58 atoms). The charge values obtained for this system (except those in the fullerene) were directly used for the FN-2a polarizer (see Table S.XIII).

Finally, for the determination of the charges in the substituent chain, various conformations of a suitable model system (see Figure S15) were DFT-optimized (Orca 4.0.1, HF/6-31g\*). As previously, the fullerene was replaced by two six-membered rings to reduce the computational demand. As expected, the all-*trans* conformation 1 is the most favourable one. Gauche conformations involving the C<sub>3</sub> chain are associated with only slightly higher energies (conformations 5-8) unless they lead to significant steric interaction of the Boc group (conformations 9 and 10). Additionally, the rotation of the entire chain (resulting in parallel orientation of both ester groups, conformation 2) and formation of a *cis*-peptide bond (conformation 4) appears to be possible at 300 K. For the ester group, the *Z*-isomer is clearly preferred (compare conformation 3).

Partial charges for the atoms in the chain substituent were obtained by RESP fitting of the conformations given in Figure S15, excluding the high-energy conformations 3 and 9. The total sum charge of the chain was constrained to  $0.25203$  e, the value for each of the methyl groups in the model system discussed above (Figure S16, right). The charges were subsequently averaged based on the Boltzmann populations of the remaining 9 conformations at 300 K, leading to the values given in Table S.XIII. For the fullerene carbon atoms in FN-2a an additive model was assumed, combining the weak electron-donating and electron-withdrawing effects of the pyrrolidine and cyclopropyl substituents, respectively (models in Figure S16). The resulting charge value was evenly distributed over all fullerene carbon atoms not directly influenced by the substitutions (46 atoms in FN-2a).

Since the precise position of the cyclopropyl substitutions on the FN-2a molecule is unknown (it is likely a mixture of different substitutions), two models with different substitution patterns were arbitrarily chosen for the MD simulations (Figure S18). The results indicate that the dynamic behavior of the nitroxide moiety - responsible for DNP - is independent on the substitution positions (Figure S18).

### S11.2.2 Bond, angle and non-bonding parameters

For chloroform, the relevant bond and angle parameters were taken from the literature [8] and translated to the Gromacs format. Parameters for the TN and FN-2a systems were built using Acpype 0.1 [5]. The parameters for the TEMPO moiety were then adjusted manually to match those specifically derived for nitroxide radicals [29]. The dummy atoms representing the nitroxide oxygen lone pairs in the original setup were omitted in our simulations.

Table S.XI: Partial charges for chloroform.

Atom	Partial charge (e)
C	$-0.16354$
Cl	$-0.03217$
H	$0.26005$

Table S.XII: Partial charges for TEMPONE, labeling of the atoms is displayed in Figure S14.

Atom	Partial charge (e)	Atom	Partial charge (e)
O1	−0.29810	C3	0.87587
O2	−0.59783	C4	−0.44168
N	−0.15144	H1	0.16391
C1	0.59983	H2	0.11526
C2	−0.65010		

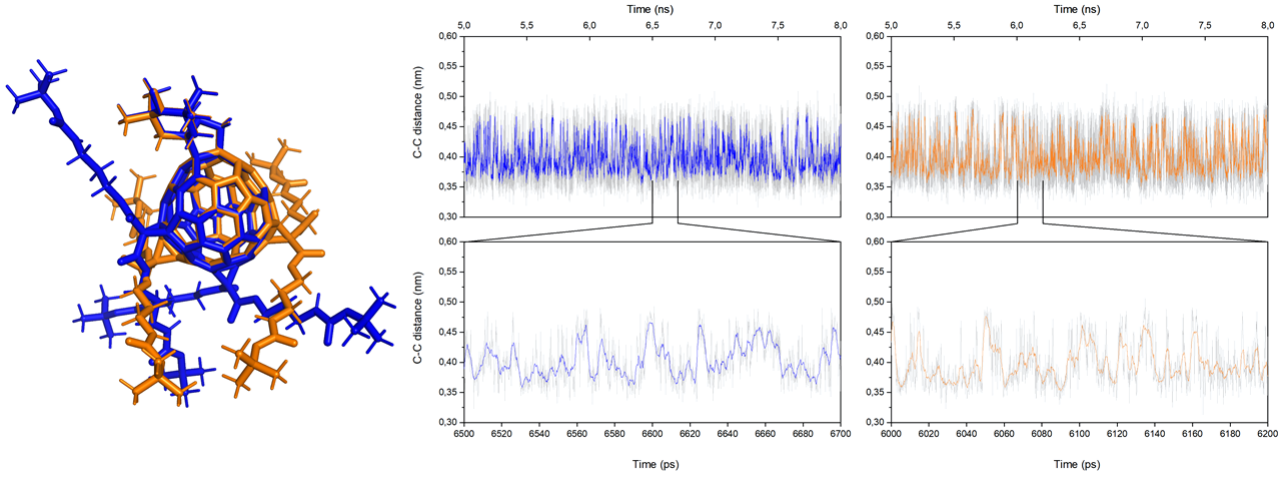


Figure S18: (Left) FN-2a molecules with different positions for the two cyclopropyl substitutions. (Right) Time traces of the C-C distance between the methyl groups on the nitroxide ring. See main text for the simulation details.

Table S.XIII: Partial charges for FN-2a. All fullerene carbon atoms except those indicated and their symmetry equivalent ones are assumed to have the same charge as C1. For atoms labels please refer to Figure S19.

Atom	Partial charge (e)	Atom	Partial charge (e)
O1	−0.27273	C11	−0.98987
O2	−0.62003	C12	1.08481
O3	−0.47427	C13	0.04027
O4	−0.61824	C14	0.06630
O5	−0.58987	C15	0.32713
N1	0.12799	C16	1.05500
N2	−0.32471	C17	0.74084
N3	−0.86661	C18	−0.45627
C1	0.00121	H1	0.28600
C2	0.40318	H2	0.18655
C3	−0.19764	H3	−0.22414
C4	0.54706	H4	0.14261
C5	−1.08335	H5	0.06602
C6	0.29144	H6	0.01557
C7	−0.71061	H7	−0.02143
C8	0.31753	H8	0.38150
C9	0.61905	H9	0.10713
C10	−0.57676		

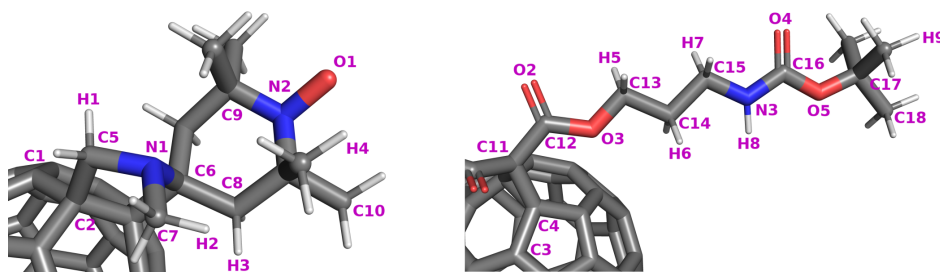


Figure S19: Atom numbering scheme for the side chain and the nitroxide group of the fullerene nitroxide.

### S11.2.3 System setup, equilibration and simulation details

All MD simulations were carried out with Gromacs 2018.4 [3, 7, 11, 25]. The polarizer molecule was placed in a pre-equilibrated box of chloroform molecules (1348 for TN, 2485 for FN-2a), energy minimized and equilibrated for 500 ps in the nvt and 500 ps in the npt ensembles, giving final densities ( $1.485 \text{ g} \cdot \text{cm}^{-3}$ ) very close to the experimental value for chloroform ( $1.49 \text{ g/cm}^3$  at  $25^\circ\text{C}$  from Sigma-Aldrich catalogue). The isothermal compressibility was matched to the literature value of  $1.01 \cdot 10^{-4} \text{ bar}^{-1}$  [27]. Simulation runs of 10 ns duration were then conducted with a temporal resolution of 200 ps. For all procedures integration steps of 2 fs were used.

## References

- [1] C. I. Bayly, P. Cieplak, W. D. Cornell, and P. A. Kollman. A well-behaved electrostatic potential based method using charge restraints for deriving atomic charges: the RESP model. *J. Phys. Chem.*, 97:10269–10280, 1993.
- [2] M. Bennati, C. Luchinat, G. Parigi, and M. T. Türke. Water  $^1\text{H}$  relaxation dispersion analysis on a nitroxide radical provides information on the maximal signal enhancement in Overhauser dynamic nuclear polarization experiments. *Phys. Chem. Chem. Phys.*, 12(22):5902–5910, 2010.
- [3] G. Bussi, D. Donadio, and M. Parrinello. Canonical sampling through velocity rescaling. *J. Chem. Phys.*, 126(1):014101, 2007.
- [4] K.-C. Chung, H.-Y. Yu, and S. Ahn. Convection effects on PGSE-NMR self-diffusion measurements at low temperature: Investigation into sources of induced convective flows. *Bull. Korean Chem. Soc.*, 32:1970–1974, 2011.
- [5] A. W. S. da Silva and W. F. Vranken. ACPYPE - AnteChamber PYthon Parser interfacE. *BMC Research Notes*, 5:367, 2012.
- [6] N. Enkin, G. Liu, M. del Carmen Gimenez-Lopez, K. Porfyrakis, I. Tkach, and M. Bennati. A high saturation factor in Overhauser DNP with nitroxide derivatives: the role of  $^{14}\text{N}$  nuclear spin relaxation. *Phys. Chem. Chem. Phys.*, 17:11144–11149, 2015.
- [7] U. Essmann, L. Perera, M. L. Berkowitz, T. Darden, H. Lee, and L. G. Pedersen. A smooth particle mesh Ewald method. *J. Chem. Phys.*, 103(19):8577–8593, 1995.
- [8] T. Fox and P. A. Kollman. Application of the RESP methodology in the parametrization of organic solvents. *J. Phys. Chem. B*, 102(41):8070–8079, 1998.
- [9] S. Grimme, J. Anthony, S. Ehrlich, and H. Krieg. A consistent and accurate ab initio parametrization of density functional dispersion correction (DFT-D) for the 94 elements H-Pu. *J. Chem. Phys.*, 132:154104, 2010.
- [10] S. Grimme, S. Ehrlich, and L. Goerigk. Effect of the damping function in dispersion corrected density functional theory. *J. Comput. Chem.*, 32:1456–1465, 2011.

- [11] B. Hess, H. Bekker, H. J. C. Berendsen, and J. G. E. M. Fraaije. LINCS: A linear constraint solver for molecular simulations. *J. Comput. Chem.*, 18(12):1463–1472, 1997.
- [12] M. Holz, S. R. Heil, and A. Sacco. Temperature-dependent self-diffusion coefficients of water and six selected molecular liquids for calibration in accurate  $^1\text{H}$  NMR PFG measurements. *Phys. Chem. Chem. Phys.*, 2:4740–4742, 2000.
- [13] L.-P. Hwang and J. H. Freed. Dynamic effect of pair correlation function on spin relaxation by translational diffusion in liquids. *J. Chem. Phys.*, 63(9):4017–4025, 1975.
- [14] A. Jerschow and N. Müller. Suppression of convection artifacts in stimulated-echo diffusion experiments. Double-stimulated-echo experiments. *J. Magn. Reson.*, 125:372–375, 1997.
- [15] D. Kruk, A. Korpala, E. Rössler, K. A. Earle, W. Medycki, and J. Moscicki.  $^1\text{H}$  NMR relaxation in glycerol solutions of nitroxide radicals: Effects of translational and rotational dynamics. *J. Chem. Phys.*, 136(11):114504, 2012.
- [16] S. E. Küçük and D. Sezer. Multiscale computational modeling of  $^{13}\text{C}$  DNP in liquids. *Phys. Chem. Chem. Phys.*, 18(18):9353–9357, 2016.
- [17] G. Liu, M. Levien, N. Karschin, G. Parigi, C. Luchinat, and M. Bennati. One-thousand-fold enhancement of high field liquid nuclear magnetic resonance signals at room temperature. *Nat. Chem.*, 9:676–680, 2017.
- [18] T. Lu and F. Chen. Multiwfn: A multifunctional wavefunction analyzer. *J. Comput. Chem.*, 33:580–592, 2012.
- [19] F. Neese. The ORCA program system. *WIREs Comput. Mol. Sci.*, 2(1):73–78, 2012.
- [20] F. Neese. Software update: the ORCA program system, version 4.0. *WIREs Comput. Mol. Sci.*, 8:e1327, 2018.
- [21] F. Neese, F. Wennmohs, A. Hansen, and U. Becker. Efficient, approximate and parallel Hartree-Fock and hybrid DFT calculations. A ‘chain-of-spheres’ algorithm for the Hartree-Fock exchange. *Chem. Phys.*, 356:98–109, 2009.
- [22] T. Orlando, R. Dervişoğlu, M. Levien, I. Tkach, T. F. Prisner, L. B. Andreas, V. P. Denysenkov, and M. Bennati. Dynamic nuclear polarization of  $^{13}\text{C}$  nuclei in the liquid state over a 10 Tesla field range. *Angew. Chem.*, 58(5):1402–1406, 2019.
- [23] G. Parigi, E. Ravera, M. Bennati, and C. Luchinat. Understanding Overhauser Dynamic Nuclear Polarisation through NMR relaxometry. *Mol. Phys.*, 117:888–897, 2018.
- [24] C. F. Polnaszek and R. G. Bryant. Nitroxide radical induced solvent proton relaxation: measurement of localized translational diffusion. *J. Chem. Phys.*, 81(9):4038–4045, 1984.
- [25] S. Pronk, S. Páll, R. Schulz, P. Larsson, P. Bjelkmar, R. Apostolov, M. R. Shirts, J. C. Smith, P. M. Kasson, D. van der Spoel, B. Hess, and E. Lindahl. GROMACS 4.5: a high-throughput and highly parallel open source molecular simulation toolkit. *Bioinformatics*, 29(7):845–854, 02 2013.
- [26] E. Ravera, C. Luchinat, and G. Parigi. Basic facts and perspectives of Overhauser DNP NMR. *J. Magn. Reson.*, 264:78–87, 2016.
- [27] A. J. Richards and K. S. Rogers. The isothermal compressibility of organic liquids by ultracentrifugation. correlation with surface tension. *Can. J. Chem.*, 49:3956–3959, 1971.
- [28] D. Sezer. Computation of DNP coupling factors of a nitroxide radical in toluene: seamless combination of MD simulations and analytical calculations. *Phys. Chem. Chem. Phys.*, 15(2):526–540, 2013.

- [29] E. Stendardo, A. Pedone, P. Cimino, M. C. Menziani, O. Crescenzi, and V. Barone. Extension of the AMBER force-field for the study of large nitroxides in condensed phases: an ab initio parameterization. *Phys. Chem. Chem. Phys.*, 12:11697–11709, 2010.
- [30] S. Stoll and A. Schweiger. EasySpin, a comprehensive software package for spectral simulation and analysis in EPR. *J. Magn. Reson.*, 178(1):42–55, 2006.
- [31] M.-T. Tuerke and M. Bennati. Saturation factor of nitroxide radicals in liquid DNP by pulsed ELDOR experiments. *Phys. Chem. Chem. Phys.*, 13:3630–3633, 2011.
- [32] P. J. M. van Bentum, G. H. A. van der Heijden, J. A. Villanueva-Garibay, and A. P. M. Kentgens. Quantitative analysis of high field liquid state dynamic nuclear polarization. *Phys. Chem. Chem. Phys.*, 13(39):17831, 2011.
- [33] F. Weigend. Accurate Coulomb-fitting basis sets for H to Rn. *Phys. Chem. Chem. Phys.*, 8:1057–1065, 2006.
- [34] F. Weigend and R. Ahlrichs. Balanced basis sets of split valence, triple zeta valence and quadruple zeta valence quality for H to Rn: Design and assessment of accuracy. *Phys. Chem. Chem. Phys.*, 7:3297–3305, 2005.
- [35] J. Winkelmann. *Self-diffusion coefficient of toluene*, volume 15B1, pages 317–319. Springer, Berlin, Heidelberg, 2017.
- [36] G. Zheng, T. Stait-Gardner, P. G. A. Kumar, A. M. Torres, and W. S. Price. PGSTE-WATERGATE: An STE-based PGSE NMR sequence with excellent solvent suppression. *J. Magn. Reson.*, 191:159–163, 2008.